LOCKHEED MARTIN ENERGY RESEARCH LIBRARIES
3 4456 0449246 7

ORNL-5291

cy. 1

Eu_2O_3: Properties and Irradiation Behavior

A. E. Pasto
M. M. Martin

OAK RIDGE NATIONAL LABORATORY
CENTRAL RESEARCH LIBRARY
DOCUMENT COLLECTION
LIBRARY LOAN COPY
DO NOT TRANSFER TO ANOTHER PERSON
If you wish someone else to see this document, send in name with document and the library will arrange a loan.
UCN-7969
(3 3-67)

OAK RIDGE NATIONAL LABORATORY
OPERATED BY UNION CARBIDE CORPORATION FOR THE ENERGY RESEARCH AND DEVELOPMENT ADMINISTRATION

Printed in the United States of America. Available from
National Technical Information Service
U.S. Department of Commerce
5285 Port Royal Road, Springfield, Virginia 22161
Price: Printed Copy $4.00; Microfiche $3.00

This report was prepared as an account of work sponsored by the United States Government. Neither the United States nor the Energy Research and Development Administration/United States Nuclear Regulatory Commission, nor any of their employees, nor any of their contractors, subcontractors, or their employees, makes any warranty, express or implied, or assumes any legal liability or responsibility for the accuracy, completeness or usefulness of any information, apparatus, product or process disclosed, or represents that its use would not infringe privately owned rights.

ORNL-5291
Distribution Categories
UC-79b, 79e

Contract No. W-7405-eng-26

METALS AND CERAMICS DIVISION

Eu_2O_3: PROPERTIES AND IRRADIATION BEHAVIOR

A. E. Pasto and M. M. Martin

Date Published: August 1977

LOCKHEED MARTIN ENERGY RESEARCH LIBRARIES
3 4456 0449246 7

OAK RIDGE NATIONAL LABORATORY
Oak Ridge, Tennessee 37830
operated by
UNION CARBIDE CORPORATION
for the
ENERGY RESEARCH AND DEVELOPMENT ADMINISTRATION

CONTENTS

ABSTRACT 1

INTRODUCTION 1

POWDER SYNTHESIS AND CHARACTERIZATION 1

FABRICATION 4

PHYSICAL AND CHEMICAL CHARACTERISTICS 4

- X-Ray Density 4
- Chemical Composition 4
- Microstructure, Hardness, and Surface Finish 7
- Thermal Expansion 8
- Thermal Conductivity and Performance 9
- Degradation in Laboratory Atmosphere 12
- Compatibility with Cladding and Coolant 13

IRRADIATION BEHAVIOR 14

- BICM-1 Experiment 15
- BICM-1 Experiment Conclusions 18
- FDOT Experiment Results 18
- FDOT Experiment Conclusions 23

SUMMARY AND RECOMMENDATIONS 24

ACKNOWLEDGMENTS 24

Eu_2O_3: PROPERTIES AND IRRADIATION BEHAVIOR

A. E. Pasto and M. M. Martin*

ABSTRACT

Europium sesquioxide is an excellent candidate control material for fast reactors. Its properties and behavior have been under extensive investigation at ORNL since 1972. This report is a compilation of the results of these efforts. Processes for synthesizing powders and fabricating dense pellets from them are described. Physical and chemical properties data measured on these pellets, along with their irradiation behavior, are also summarized.

INTRODUCTION

Europium sesquioxide (Eu_2O_3) is a fast neutron absorber material that is receiving consideration for use in Liquid Metal Fast Breeder Reactors (LMFBRs) in the United States, Great Britain, Germany, Russia, and France. At ORNL, investigation of the properties of Eu_2O_3 for potential U.S. application dates from 1972. This document presents the results of our studies on synthesis, fabrication, physical and chemical attributes, compatibility with stainless steel cladding and sodium coolant, and irradiation behavior of europia. Specific nuclear aspects such as macroscopic worth and heat generation rate have been discussed elsewhere,[1-5] and will not be dealt with here.

POWDER SYNTHESIS AND CHARACTERIZATION

Europium sesquioxide may exist in two potentially useful forms: a cubic phase stable from ambient up to about 1050°C, and a monoclinic phase stable from ambient up to about 2040°C. The cubic phase is obtained in Eu_2O_3 powders by calcination of compounds which decompose at temperatures below 1050°C. If cubic powder is then heated above this temperature, it transforms to a monoclinic phase. The transition is irreversible under normal conditions,[6-8] but apparently can be reversed under sufficient pressure.[9,10]

*Work performed under ERDA/RRD 189a No. OH029, Advanced Absorber Materials.

1. A. E. Pasto, *Europium Oxide as a Potential LMFBR Control Material,* ORNL/TM-4226, Oak Ridge (September 1973).
2. R. J. Tuttle and T. H. Springer, "Reactivity Worths of Boron, Tantalum, and Europium in a Fast Reactor Spectrum," *Nucl. Sci. Eng.* 49: 468–81 (1972).
3. E. L. Gluekler, pp. 7-1 through 7-6 in *Core Engineering, Forty-Ninth Quart. Rept. Nov. 1973–Jan. 1974,* GEAP-10028-49, Advanced Technology Dept., General Electric Co., Sunnyvale, Calif. (February 1974).
4. H. Takahashi, *Evaluation of the Neutron and Gamma-Ray Production Cross Sections of* ^{151}Eu *and* ^{153}Eu, BNL-19455 (ENDF-213), Brookhaven National Laboratory, Upton, N.Y. (November 1974).
5. E. L. Gluekler, pp. 7-4 through 7-7 in *Core Engineering, Fiftieth Quart. Rept. Feb.–April 1974,* GEAP-10028-50, Advanced Technology Dept., General Electric Co., Sunnyvale, Calif. (May 1974).
6. S. Stecura, *Crystallographic Modifications and Phase Transformation Rates of Five Rare Earth Sesquioxides,* U.S. Bureau of Mines Report of Investigations 6616 (1964).
7. R. S. Roth and S. J. Schneider, "Phase Equilibria in Systems Involving the Rare Earth Oxides. Part I. Polymorphism of the Oxides of the Trivalent Rare-Earth Ions," *J. Res. Nat. Bur. Stand.* 64A(4): 309–16 (1960).
8. G. Brauer, "Precipitation of Rare Earth Oxides from Molten Salts," pp. 385–90 in *Proc. 6th Rare Earth Res. Conf., Gatlinburg, Tenn.* (1967).
9. I. Warshaw and R. Roy, "Polymorphism of the Rare Earth Sesquioxides," *J. Phys. Chem.* 65: 2048–51 (1961).
10. H. R. Hoekstra, "Phase Relationships in the Rare Earth Sesquioxides at High Pressure," *Inorg. Chem.* 5(5): 754–57 (1966).

The monoclinic phase possesses the advantages of a higher europium atom density (higher worth per unit volume), and phase stability through a larger temperature range. The cubic material offers the possibility of better irradiation performance because of its isotropic structure. However, its low upper use temperature and nuclear worth have limited its consideration, and the bulk of the effort has been expended on the monoclinic material.

Most commercially available powders are of the cubic phase, requiring a heat treatment to transform them to the monoclinic phase. Our developed fabrication procedures, described later, allow conversion to take place during densification.

One high-purity commercially available[11] cubic powder, which sinters more readily than others into dense compacts, comprised the bulk of the raw material utilized for our experiments. Table 1 contains the results of our characterization of a typical sample of this product.

Because of the 0.5% weight loss consisting primarily of adsorbed CO_2 and/or H_2O, the as-received powder requires preparation before consolidation. Calcination in air for 3 hr at 1000°C in high-purity Al_2O_3 crucibles significantly reduces these volatile contaminants. Storage of the calcined powder in glass bottles under vacuum or dry argon adequately maintains the resultant purity.

As shown in Table 1, the calcining treatment causes an expected reduction in specific surface area and an increase in particle size. However, examination of the particles before and after calcination (Fig. 1)

11. Molycorp Product Code 5000, 99.99% purity, from Molybdenum Corp. of America, White Plains, N.Y.

Table 1. Characterization of cubic Eu_2O_3 powder

Element or characteristic	As received	As calcined
Chemical analysis[a] (wt ppm)		
Al	6	6
B	8	8
Ca	10	30
Cl	400	400
Cu	2	2
Fe	250	10
K	3	3
Mg	<6	<6
Mn	1	<0.3
Mo	<3	<3
Na	5	2
Ni	2	2
P	2	2
Pb	<3	<3
S	20	5
Si	<10	<10
Zn	300	300
Zr	<1	<1
Re	<10	<10
Eu content (wt %)	86.22	Not determined
Physical analysis		
Loss on ignition (wt % at 1000°C)	0.512	0.071
Surface area (m^2/g)	6.64	3.95
Particle size (μm)		
90 wt % less than	3.5	10.9
50 wt % less than	1.7	4.8
10 wt % less than	0.6	2.0

[a]Determined by spark source mass spectroscopy.

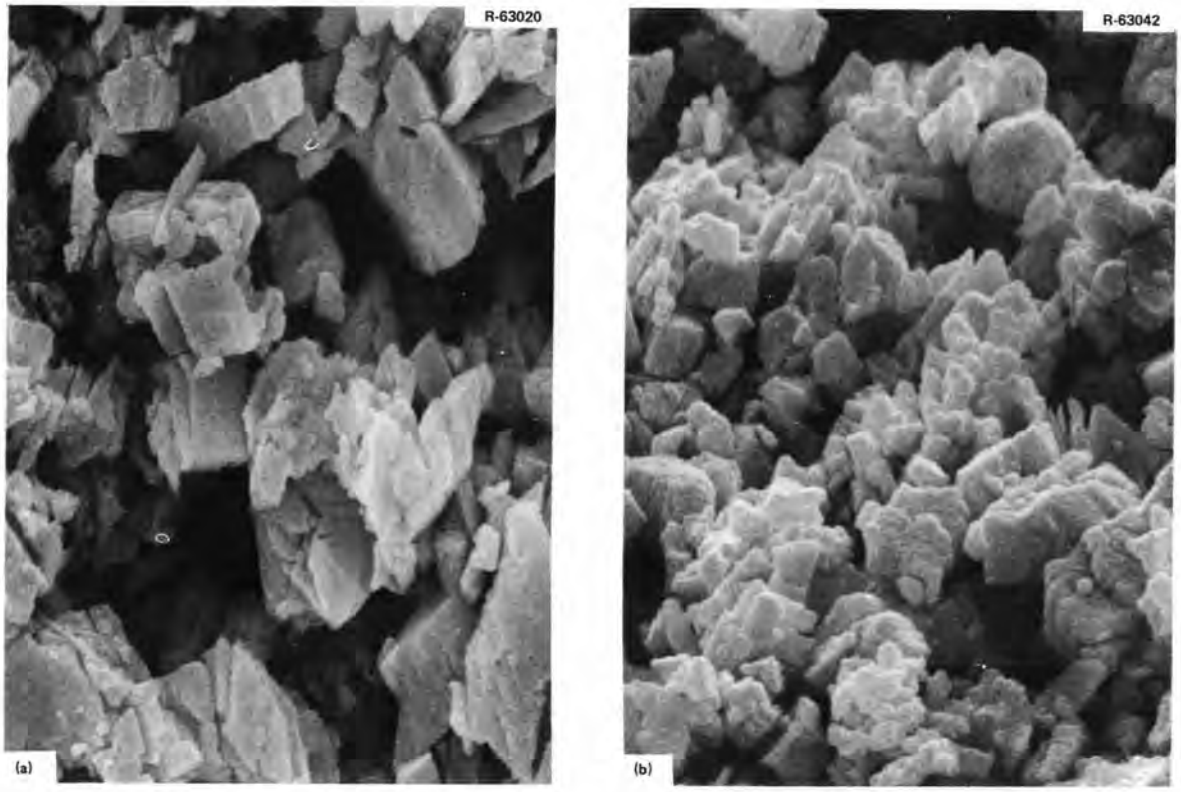

Fig. 1. Scanning electron micrographs of cubic phase Eu_2O_3 powder. (a) As received, (b) as calcined. 3000×. Reduced 39%.

shows that in fact the calcined powder consists of smaller crystallites, perhaps formed by breaking up of the larger ones when the volatile species were removed. The larger particle sizes reported in Table 1 are then not truly representative of the powder crystallite size, but represent loosely sintered agglomerates.

Powders were also prepared from chemically reprocessed scrap material. Preparation entailed precipitation from nitric acid solutions as hydroxide or oxalate, followed by calcination at various temperatures. Although hydroxide-derived powders had higher surface areas than commercially obtained or oxalate-derived powders, they did not sinter to densities as high as the latter.[12] This observation perhaps indicates that the derivation of the powder is the reason for the difference in sinterability of essentially identical commercial powders. Our oxalate-derived europia calcined at 900°C and pressed to equivalent green densities yielded sintered pellets of grain size and density identical to those of the best commercial material.[13,14] However, because of the higher purity routinely obtained with commercial powders, commercial material was utilized for the remainder of the experiments described.

---

12. A. E. Pasto, *Fuels and Materials Development Program Quart. Progr. Rept. for Period Ending Dec. 31, 1974*, ORNL/TM-4878, pp. 4–5, Oak Ridge (April 1975).

13. A. E. Pasto and D. E. LaValle, *Fuels and Materials Development Program Quart. Progr. Rept. for Period Ending June 30, 1974*, ORNL/TM-4688, pp. 6–9, Oak Ridge (October 1974).

14. A. E. Pasto, *Fuels and Materials Development Program Quart. Progr. Rept. for Period Ending Sept. 30, 1974*, ORNL/TM-4726, pp. 3–5, Oak Ridge (January 1975).

FABRICATION

The qualification of europia for reactor use includes irradiation testing. Current control rod designs require the material to be in the form of cylindrical pellets with as high a density as practical, in excess of 90% of theoretical. Hence we investigated sintering and hot-pressing techniques for pellet fabrication. Since europium sesquioxide is subject to reduction[15] to Eu_3O_4 in highly reducing environments and may be subject to a prohibitive limiting density when sintered in inert atmospheres, high-vacuum furnaces[16] were utilized for the fabrication work. Complete results of this part of the program have been reported elsewhere.[17] In general, uniaxial pressing of cubic Eu_2O_3 powders at pressures of 10,000 to 20,000 psi (69 to 138 MPa), without use of a binder, yielded pellets with green densities of 45 to 47% of theoretical. These preforms were sintered at 1650°C for 3 hr in vacuum without formation of cracks; and the resultant monoclinic bodies after subsequent calcination in air at 1000°C exhibit 94 to 96% of theoretical density, with an average grain size of about 20 μm. This is true for both the commercial and the calcined oxalate-derived material.

Alternatively, vacuum hot-pressing was found to be a means of obtaining either higher density (up to 100%, but with larger grain size) or smaller grain size at equivalent sintered density in monoclinic products. Further, pellets of the lower-temperature cubic phase could be produced with densities of 92% of theoretical by hot-pressing below the phase transformation temperature.

PHYSICAL AND CHEMICAL CHARACTERISTICS

Several hundred pellets have been produced by the described methods. More than 200 were utilized in irradiation tests to be described later, and these were subjected to extensive pretest characterization. To facilitate presentation of results, Table 2 describes the consolidation of pellets designated types A through F. The A, C, and D types are sintered monoclinic oxide; B and E are hot-pressed cubic oxide; and F is hot-pressed monoclinic phase material.

X-Ray Density

Specimens from one to two pellets of each type were analyzed by x-ray diffraction. The technique employed a Debye-Scherrer powder camera of diameter 114.6 mm, a vanadium-filtered chromium Kα x-ray beam with an average α_1 and α_2 wave length of 2.29092 Å, and least squares extrapolation for calculation of lattice parameters. Results are presented in Table 3; values in parentheses are standard deviations for the lattice parameters and standard errors for calculated densities, both for the last digit. Based on these measurements, the average x-ray densities for monoclinic and cubic Eu_2O_3 fabricated as outlined in Table 2 are respectively 7.952 and 7.289 g/cm^3.

Chemical Composition

Results of chemical analyses on one to two pellets of each type are given in Table 4. All samples exhibited similar europium and oxygen contents, in stoichiometric proportions expected for Eu_2O_3.

---

15. G. J. McCarthy, "Oxygen-Fugacity-Temperature Diagram for the Eu-O System," *J. Amer. Ceram. Soc.* 57(11): 502 (1974).

16. Models 424B, 424C, and 426 Vacuum/Inert Gas Furnaces from Richard D. Brew and Co., Inc., Concord, N.H.

17. A. E. Pasto, M. M. Martin, and R. G. Donnelly, "Vacuum Sintering and Hot Pressing of Eu_2O_3," pp. 14–22 in *Proc. 11th Rare Earth Res. Conf., Oct. 7–10, 1974,* CONF-741002-P1 (1974).

Table 2. Attributes and parameters of consolidation of Eu_2O_3 preforms

Description	Type of preform					
	A	B	C	D	E	F
Green compacting parameters						
Number produced	53	27	37	100	54	45
Technique	Sintering	Hot-pressing	Sintering	Sintering	Hot-pressing	Hot-pressing
Die and punch material	AISI A6 steel	ATJ graphite	AISI A6 steel	AISI A6 steel	ATJ graphite	ATJ graphite
Die lubricant	Stearic acid + acetone	None	Stearic acid + acetone	Stearic acid + acetone	None	None
Pressed to height	Yes	No	Yes	Yes	No	No
Nominal green compacting attributes						
Diameter, in. (mm)	0.801(20.32)	0.578(14.68)	0.928(23.57)	0.928(23.57)	0.680(17.27)	0.680(17.27)
Length, in. (mm)	1.47(37.3)	~4.6(117)	1.74(44.2)	1.75(44.4)	~5.3(135)	~6.4(163)
Density, % of theoretical	44.4	~25	45.4	44.6	~25	~25
Final densifying conditions[a]						
Number of preforms per furnace run	8 and 9	9	6	6 and 16	9	9
Sintering boat or hot-pressing die material	Molybdenum	ATJ graphite	Molybdenum	Molybdenum	ATJ graphite	ATJ graphite
Heating element material	Tungsten	Graphite	Tungsten	Graphite and tungsten	Graphite	Graphite
Applied pressure, psi (MPa)	*b*	~6000(41)	*b*	*b*	~6000(41)	~6000(41)
Initial heating rate, °C/hr	~500 to 1000	~500 to 500	~400 to 800	~400 to 800	~500 to 500	~550 to 1125[c]
Final heating rate, °C/hr	~650 to 1650	~500 to 1020	~950 to 1750	~800 to 1650	~500 to 1020	~1000 to 1300
Duration at temperature, hr	3 at 1650°C	3 at 1020°C	3 at 1750°C	3 at 1650°C	3 at 1020°C	1 at 1300°C
Cooling rate, °C/hr	~650 to 1000	*b*	~750 to 1000	~650 to 1000	*b*	*b*
Nominal preform attributes						
Diameter, in. (mm)	0.598(15.19)	0.575(14.60)	0.692(17.58)	0.695(17.65)	0.677(17.20)	0.678(17.22)
Length, in. (mm)	1.12(28.4)	1.27(32.3)	1.33(33.8)	1.34(34.0)	1.47(37.3)	1.54(39.1)
Density, % of theoretical	94.3	90.5	95.9	94.3	90.1	94.6

[a]Under vacuum of 10^{-4} torr (13 mPa).
[b]Not applicable.
[c]Held at 1125°C for 50 min.

Table 3. Lattice parameters and x-ray densities of Eu_2O_3 pellets[a]

Type of pellet	Lattice parameters				X-ray density (g/cm^3)
	a_0 (Å)	b_0 (Å)	c_0 (Å)	β (deg)	
			Monoclinic[b]		
A	14.1129 (9)	3.6023 (1)	8.8073 (4)	100.029 (5)	7.952 (7)
C	14.1103 (8)	3.6022 (1)	8.8086 (3)	100.029 (5)	7.953 (7)
D	14.1146 (8)	3.6025 (1)	8.8144 (7)	100.039 (5)	7.948 (8)
D	14.1081 (9)	3.6023 (1)	8.8084 (4)	100.037 (6)	7.954 (8)
F	14.1126 (13)	3.6026 (2)	8.8076 (15)	100.045 (11)	7.952 (15)
			Cubic[c]		
B	10.8652 (4)				7.2897 (8)
E	10.8658 (4)				7.2885 (8)

[a]Standard errors for the last digit are given in parentheses.
[b]Six "molecules" per unit cell.
[c]Sixteen "molecules" per unit cell.

Table 4. Results of chemical analyses on Eu_2O_3 pellets

Type of pellet	Composition, wt %		Detected impurities				
	Europium	Oxygen	Moisture (wt ppm)	Gaseous compounds	Gas (cm^3/g at STP)	Elements: Major[a]	Elements: Minor[b]
A	86.2	14.0	20	H_2, N_2+CO	0.02	None	C,Fe
B	86.1	14.1	400	CO_2	0.1	C,Cl,S,Zn	Al,Fe,Si
C	86.2	13.9	6	H_2, N_2+CO	0.02	None	C,Fe
D	86.2	13.8	10	H_2, N_2+CO	0.01	None	C,Fe,Si
D	86.4	13.2	20	H_2, N_2+CO	0.02	None	C
E	86.4	13.8	300	CO_2	0.1	C,S,Zn	None
E	86.5	13.8	315	CO_2	0.2	C,Cl,S,Zn	None
F	86.1	14.0	<1		0.004	None	C,Cr,Fe,Zn

[a]Represents range between 100 and 500 wt ppm.
[b]Represents range between 20 and 100 wt ppm.

Cubic-phase pellets (types B and E) exhibited maximal moisture and gas contents of about 400 wt ppm and 0.2 cm^3/g at STP respectively. This gas was predominantly CO_2. The pellet fabrication temperature of 1020°C failed to reduce the chlorine, sulfur, and zinc contents of the starting powder below 100 wt ppm. In comparison, the monoclinic structure specimens (types A, C, D, and F) contained no major impurity elements, and their moisture and gas contents were an order of magnitude lower than for the cubic structure specimens.

The predominant gas species evolved from the sintered monoclinic structure pellets was N_2 + CO, undoubtedly adsorbed on the pellet surface. The residual carbon content of all pellets was in the range of about 50 to 150 wt ppm, with the cubic structure pellets containing the slightly larger amounts. This may be due to the inclusion of carbon from the adsorbed CO_2 into the total carbon value.

Microstructure, Hardness, and Surface Finish

One pellet of each type was examined ceramographically to determine microstructure, grain size, and microhardness. Results of the physical measurements are given in Table 5. Figure 2 shows the appearance of polished and etched specimens of hot-pressed cubic, hot-pressed monoclinic, and two types of sintered monoclinic materials. The etchant of lactic-nitric-hydrochloric acid solution successfully used for monoclinic Eu_2O_3 failed to delineate the grain structure of cubic Eu_2O_3. Figure 2(a) does illustrate, however, the distribution of porosity in the pellet. The denser portions are relics of the granules derived from the prepressing and crushing operations used to prepare the starting powder. The dark areas between these relics indicate regions of higher porosity. The hot-pressed monoclinic specimen [Fig. 2(b)] also contains some of this concentrated porosity, but to a much lesser extent. The grains of this hot-pressed specimen are relatively small and equiaxed as compared with sintered type pellets A, C, and D (Table 5).

Table 5. Results of some physical measurements on ceramic Eu_2O_3 pellets

Type of pellet	Hardness (DPH)	Surface finish		Grain size	
		(μin.)	(μm)	Average diameter (μm)	Grains per mm^2 at 1X
A	160–170	170	4.3	16	4,000
B	250–350	70	1.8	*a*	*a*
C	140–160	220	5.6	27	1,400
D	160–200	150	3.8	13	5,600
E	300–400	40	1.0	*a*	*a*
F	270–290	50	1.3	8	16,000

[a]Grains were not delineated.

The two sintered monoclinic specimens [Fig. 2(c) and (d)] show the effect of sintering temperature on grain size (that is, the higher sintering temperature produces the larger grains). These photomicrographs also depict intergranular cracks of up to several hundred micrometers which constitute a manifestation of the granulating process for the starting powder. This microcracked microstructure is thought to be potentially more thermally shock-resistant and more resistant to crack propagation than an uncracked structure. It is produced by cold-pressing the calcined cubic Eu_2O_3 powder into slugs at 20,000 psi (138 MPa) and crushing the slugs to pass a 20-mesh sieve before repressing and sintering. The microcracked microstructure can be eliminated by crushing the slugs to pass a 100-mesh or finer screen.[18] The resultant uncracked pellets also have slightly higher densities than those with internal cracks. Twinning of grains, which is common in Eu_2O_3, may also be seen in Fig. 2(d).

Diamond-pyramid hardness values are reported in Table 5 for a 1000-g load on the indenter. They were greatest for cubic and monoclinic Eu_2O_3 (B, E, and F types) consolidated by our hot-pressing procedures. The relatively high value for hardness of these types, about 300 DPH, resulted in the selection of diamond-impregnated resin wheels for machining them to desired dimensions. The softer sintered pellets were ground to size with less expensive silicon carbide wheels.

Table 5 lists root-mean-square values of surface finish of machined pellets, measured with a profilometer. Smoothest surfaces were obtained for hot-pressed pellets, which had been ground with diamond wheels and possessed the smallest grain sizes and the highest hardnesses.

18. A. E. Pasto, *Fuels and Materials Development Program Quart. Prog. Rept. for Period Ending March 31, 1974*, ORNL/TM-4620, pp. 7–9, Oak Ridge (July 1974).

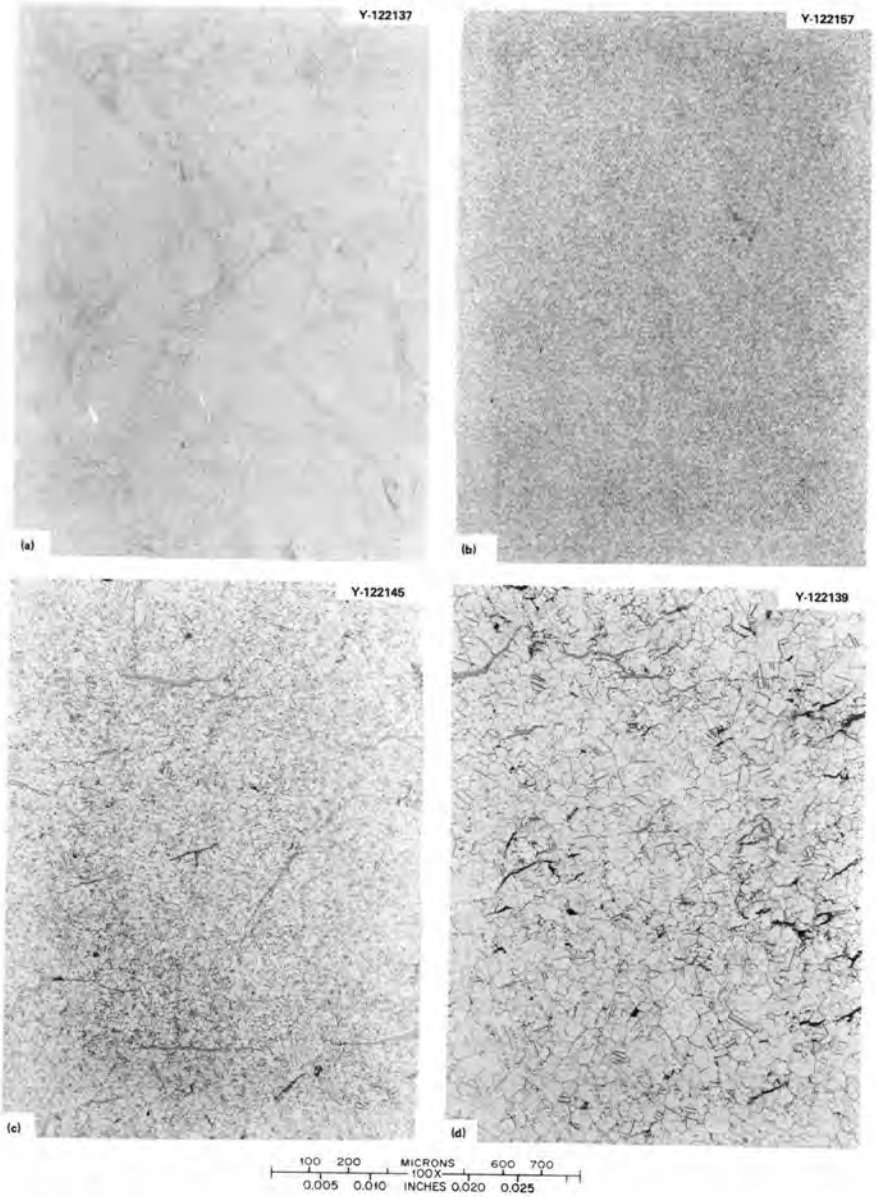

Fig. 2. Polished and etched Eu_2O_3 specimens fabricated for the design-oriented irradiation test in EBR-II. 100×. Reduced 50%. (a) Hot-pressed cubic pellet, type B. (b) Hot-pressed monoclinic pellet, type F. (c) 1650°C-sintered monoclinic pellet, type D. (d) 1750°C-sintered monoclinic pellet, type C.

Thermal Expansion

The linear thermal expansion of two specimens of sintered monoclinic europia that were prepared similarly to type A in Table 2 and then air-calcined at 1000°C was measured in an argon atmosphere. The technique employed a pushrod dilatometer, a heating rate of 2°C/min, and a platinum standard that indicated measuring error to be <1%. From 20 to 1000°C the pushrod employed was quartz, and from 20 to 1500°C Al_2O_3 was used. Length changes as a function of temperature are presented in Table 6 along with a comparison with similar data reported by Wilfong et al.[19] in 1963. Differences between the two sets

19. R. L. Wilfong, L. P. Domingues, L. R. Furlong, and J. A. Finlayson, "Thermal Expansion of the Oxides of Yttrium, Cerium, Samarium, Europium, and Dysprosium," U.S. Bureau of Mines Report of Investigations 6180 (1963).

Table 6. Linear thermal expansion of monoclinic europium oxide

Temperature (°C)	Expansion, %	
	Present results	Wilfong's data[a]
20	0	0
100	0.0582	0.0695
200	0.1457	0.1590
300	0.2341	0.2576
400	0.3255	0.3532
500	0.4193	0.4591
600	0.5157	0.5658
700	0.6160	0.6710
800	0.7192	0.7831
900	0.8259	0.8928
1000	0.9370	1.0073
1100	1.054	
1200	1.163	
1300	1.269	
1400	1.366	
1500	1.431	

[a]Data from R. L. Wilfong, L. P. Domingues, L. R. Furlong, and J. A. Finlayson, "Thermal Expansion of the Oxides of Yttrium, Cerium, Samarium, Europium, and Dysprosium," Bureau of Mines Report of Investigations 6180 (1963).

of data do not appear large; an average coefficient of thermal expansion from ambient to 1000°C for Wilfong's data is $10.35 \times 10^{-6}/°C$, whereas we obtain $9.56 \times 10^{-6}/°C$ – a difference of about 7.6%. Extrapolation of Wilfong's data gives an average coefficient to 1500°C of about $10.44 \times 10^{-6}/°C$, whereas our results give $9.67 \times 10^{-6}/°C$ – a difference of about 7.4%.

Thermal Conductivity and Performance

Thermal conductivity measurements have been made at ORNL[20] on monoclinic europia ceramics to very high precision in radial and longitudinal heat flow apparatuses. Results are presented in Table 7 and shown graphically in Fig. 3, for high-purity hot-pressed monoclinic Eu_2O_3. These recently acquired data, along with Gibby's[21] values for the cubic phases, were empirically fitted to equations of the form:

$$\lambda = (A + BT)^{-1} + CT^3 \quad , \tag{1}$$

where λ = thermal conductivity in $W\ m^{-1}\ K^{-1}$ and T = temperature in K. Values of A, B, and C are given in Table 8. This relationship for monoclinic Eu_2O_3 would be expected if both phonons and photons contributed significantly to the thermal conductivity at elevated temperature.

In comparison to many dense ceramics, both polymorphs of europia possess relatively low conductivities. We expected that this would cause formation of thermal-stress-induced cracks in

20. T. G. Godfrey, *Fuels and Materials Development Program Quart. Progr. Rept. for Period Ending Dec. 31, 1974*, ORNL/TM-4878, pp. 1–4, Oak Ridge (April 1975).

21. R. L. Gibby, *Thermal Properties of B_4C and Eu_2O_3*, HEDL-SA-587, Hanford Engineering Development Laboratory, Richland, Wash. (October 1973).

Table 7. Thermal conductivity of monoclinic Eu_2O_3 measured in three apparatuses

Temperature (K)	Thermal conductivity, W m^{-1} K^{-1}		
	λ_m	λ_{TD}[a]	λ_{TD}[b]
	Low-temperature longitudinal		
87.794	8.022	9.463	9.943
100.890	6.129	7.230	7.597
145.599	4.639	5.472	5.750
196.665	3.558	4.197	4.410
272.433	2.907	3.429	3.603
302.976	2.705	3.191	3.353
336.714	2.539	2.995	3.147
	Comparative heat flow		
303.48	2.924	3.204	
323.07	2.842	3.114	
343.46	2.751	3.014	
363.12	2.677	2.933	
	Radial heat flow		
312.06	2.959	3.199	
343.16	2.792	3.019	
368.64	2.712	2.933	
427.60	2.538	2.744	
549.02	2.257	2.440	
549.50	2.255	2.438	
661.32	2.073	2.241	
549.20	2.256	2.439	
763.17	1.946	2.104	
763.58	1.937	2.094	
842.10	1.872	2.024	
862.75	1.859	2.010	
882.55	1.843	1.992	
882.45	1.844	1.994	
882.59	1.846	1.996	
902.34	1.826	1.974	
902.48	1.839	1.989	
922.74	1.821	1.969	
942.38	1.810	1.957	
959.50	1.782	1.927	
978.61	1.780	1.924	
997.78	1.766	1.909	
763.42	1.962	2.122	
1045.62	1.746	1.887	
1091.98	1.724	1.864	
1133.88	1.716	1.855	
1209.74	1.748	1.890	
763.46	2.033	2.198	
550.04	2.366	2.558	
343.69	2.983	3.225	
764.08	2.038	2.204	

[a] $\lambda_{TD} = \lambda_m (1+P/2)/(1-P)$, where λ_m = measured conductivity, λ_{TD} = conductivity at theoretical density, and P = volume fraction porosity.

[b] $\lambda_{TD} = \lambda_m(1+P)/(1-P)$, where λ_m = measured conductivity, λ_{TD} = conductivity at theoretical density, and P = volume fraction porosity.

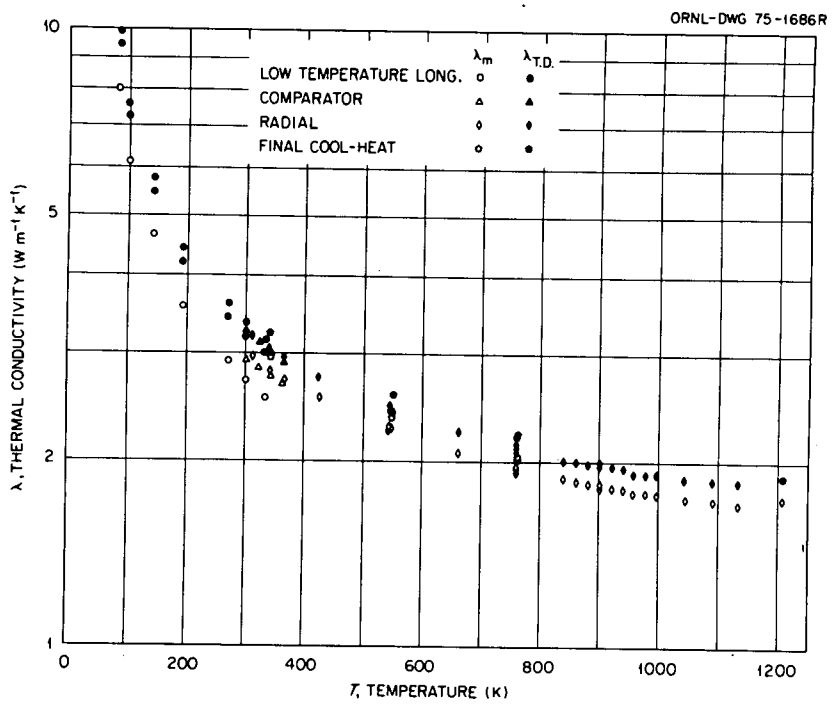

Fig. 3. Thermal conductivity of monoclinic Eu_2O_3.

Table 8. Constants for the thermal conductivity equation, $\lambda = (A + BT)^{-1} + CT^3$

Phase	A	B	C
Cubic	0.159	2.40×10^{-4}	0
Monoclinic	0.191	4.10×10^{-4}	2.19×10^{-10}

large-diameter pellets when they are subjected to high internal heat generation in an operating reactor core. To investigate the consequences of such cracking, a thermal performance test was devised. A stack of annular europia pellets was heated by an axially-located tungsten rod. Exterior pellet surface temperatures were controlled by a water-cooled heat sink surrounding a stainless steel pellet sheath. Power was applied to the tungsten core to heat the pellets at a rate of about 125°C/min to a predetermined maximum temperature. Transient heat conduction calculations were performed to provide a model for the system, which allowed the thermal conductivity of the pellet to be monitored as the temperature was cycled.

Only sintered, 0.63-in.-diam (1.60-cm) monoclinic pellets were tested. They were fabricated similarly to those produced for the irradiation tests so that performance in the test would closely simulate performance in the reactor. Results can be summarized as follows:[22]

1. In one experiment where the pellets reached about 1200°C on the inner surface, radial cracks appeared in each pellet of the stack. Some nonradial cracks also became evident, especially on dye-penetrant

22. T. G. Godfrey, O. L. Kirkland, and R. K. Williams, *Fuels and Materials Development Program Quart. Prog. Rept. for Period Ending March 31, 1975,* ORNL/TM-4940, pp. 3–5, Oak Ridge (July 1975).

testing. These are shown clearly in Fig. 4. However, there was no gross disintegration or powdering of the pellets and hence no mechanical interaction with the stainless steel pellet sheath.

2. Another experiment involved 20 cycles of heating to 1200°C and cooling. Again, cracks appeared, similar in nature to those in the previous test, as shown in Fig. 5.
3. A third experiment included 22 cycles of heating and cooling. Again the pellets remained intact, and calculations showed <1% decrease in the effective pellet thermal conductivity, even with the cracks present.

The performance test adequately predicted the behavior of large-diameter monoclinic pellets during irradiation. That is, as will be described later, the irradiated product exhibited similar appearing surface cracks. However, the most significant result that pertains to performance of a neutron absorber material is that these experiments revealed a total lack of pellet disintegration or pellet-cladding mechanical interactions when the pellets were subjected to a radial temperature gradient up to 1045°C/cm (4780°F/in.).

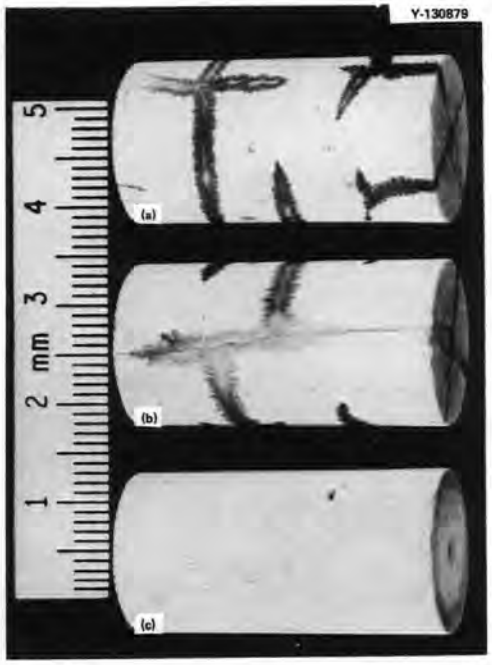

Fig. 4. Dye-penetrant test of Eu_2O_3 pellet from run 2. (a) and (b) Pellet viewed from opposite sides. (c) Penetrant-tested control pellet.

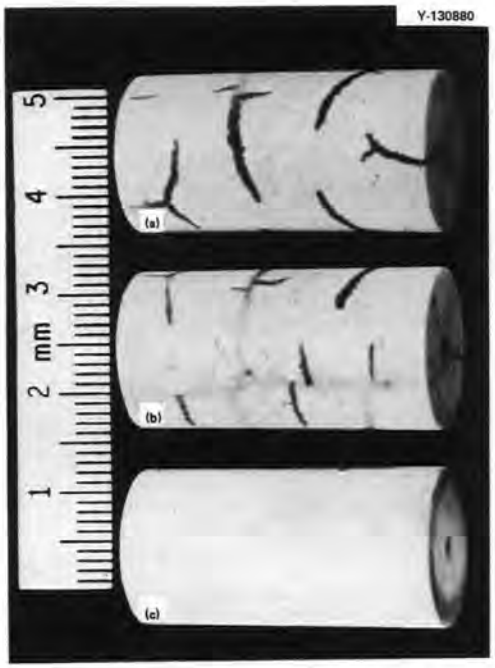

Fig. 5. Dye-penetrant test of Eu_2O_3 pellet from run 3. (a) and (b) Pellet viewed from opposite sides. (c) Penetrant-tested control pellet.

Degradation in Laboratory Atmosphere

Lanthanide oxides are susceptible to adsorption of water vapor from ambient atmospheres; this process typically results in degradation of fabricated pellets. For instance, visual examination of sintered monoclinic Eu_2O_3 pellets after exposure to ambient conditions for ten months revealed extensive swelling and cracking in some cases. The effect was manifested by weight and dimensional increases, cracking, and a resultant bulk density decrease. The magnitude of the changes appeared to be related to the initial size of the pellet, with larger pellets having larger subsequent changes. Some 0.3-in.-diam, 0.3-in.-long (8 X 8 mm)

pellets showed no cracks after two years, while several 0.63-in.-diam, 1.31-in.-long (16 X 33.3 mm) pellets exhibited cracking in as short a period as six months. A further observation was that the effect was much larger for pellets of lower initial oxygen content – that is, those that were vacuum sintered and not calcined in air at 1000°C.

The swelling and cracking behavior of other lanthanide oxides has been documented by other investigators. Fullam and Roberts[23] exposed Nd_2O_3 and Sm_2O_3 shapes to atmospheric moisture and found complete pellet disintegration. Qualitatively they found that the rates of disintegration decreased in the order $Nd_2O_3 > Pm_2O_3 > Sm_2O_3$, that is, according to decreasing cation radius. Further, they indicated that the cubic oxides react with atmospheric water vapor faster than the high-temperature forms. X-ray diffraction and thermogravimetric analysis indicated that the products formed on reaction with water or water vapor were hydrated oxides ($R_2O_3 \cdot 3H_2O$), and not hydroxides [$R(OH)_3$]. Touret and Queyroux,[24] on the other hand, found the reaction products with Sm_2O_3 and Gd_2O_3 to be hydroxides. Their observations on rates of reaction were qualitatively similar to those of Fullam and Roberts: for example, they found that the smaller the cation radius, the slower the reaction, and that the cubic oxide form reacted faster than the higher-temperature form.

It appeared that our europium oxide pellets were reacting with atmospheric water vapor to form either a hydrated oxide or hydroxide on the surface, and that the diffusion of reactant through this layer controlled the reaction rate. The reaction product was less dense than the oxide, and it caused swelling and cracking of the europia ceramic. Specifics of this reaction were not determined. Exposure of pellets to laboratory atmosphere was avoided as much as possible, or the pellets were calcined at ~1000°C in air before use.

Compatibility with Cladding and Coolant

The envisioned control rod application of Eu_2O_3 in the U.S. fast reactors involves dense cylindrical pellets encapsulated in type 316 stainless steel tubes that are cooled with flowing liquid sodium. Helium will serve as the internal heat transfer medium but sodium may contact the pellets if the cladding is breached. A primary consideration in the useful lifetime of such an absorber assembly, aside from the progressive decrease in nuclear worth, is the compatibility of the oxide with the cladding and intruding sodium.

Tests of hot-pressed cubic and both hot-pressed and sintered monoclinic Eu_2O_3 in contact with type 316 stainless steel in an argon atmosphere have recently been completed.[25,26] Exposure times ranged up to 10,000 hr at temperatures of 650, 760, and 870°C. Similar tests with sodium in contact with both Eu_2O_3 and type 316 stainless steel materials have also been concluded for times up to 1000 hr[25] at the former two temperatures. Results can be summarized as follows:

1. In the argon atmosphere, no significant reaction occurred between the stainless steel and oxide at temperatures of 760°C or below. At 870°C some reaction occurred in the steel along grain boundaries

23. H. T. Fullam and F. P. Roberts, *Reactions of the Sesquioxides of Pm, Nd, and Sm with Water,* BNWL-1421, Battelle Northwest Laboratories, Richland, Wash. (1970).

24. D. Touret and F. Queyroux, "Sur la réactivité vis-à-vis de l'eau de l'oxyde de lanthane et de quelques matériaux réfractaires à base d'oxyde de lanthane," *Rev. Chim. Miner.* 9: 883–903 (1972).

25. J. R. DiStefano, *Compatibility of Eu_2O_3 with Type 316 Stainless Steel and Sodium,* ORNL/TM-4780, Oak Ridge (January 1975).

26. J. R. DiStefano, *Liquid Metal Fast Breeder Reactor Materials Development Program Quart. Progr. Rept. for Period Ending Sept. 30, 1975,* ORNL-5117, pp. 155–58, Oak Ridge (February 1976).

when it was exposed to the hot-pressed monoclinic material. A europium-rich phase was observed in these grain boundaries. Depth of penetration was proportional to the one-half power of time, indicating a diffusion-controlled process for the reaction mechanism.

2. Tests of Eu_2O_3 with sodium and stainless steel for 1000 hr at 650 and 760°C also showed no evidence of reaction with the steel. However, sodium had reacted with the sesquioxide, leading to pellet weight increases and swelling. These effects were temperature-dependent, increasing with increasing temperatures. The process whereby sodium penetrated into the pellets indicated that the penetration was clearly related to the pellet density and microstructure (grain size), as illustrated in the micrographs in Fig. 6. The larger-grain-size material (cold-pressed and sintered) was penetrated along grain boundaries to a greater extent than the smaller grained hot-pressed material.

Since the oxide-steel contact design temperature in actual use is not expected to exceed 760°C, we conclude that helium-bonded europium sesquioxide absorber assemblies will not be degraded in design lifetime by any compatibility effects. Similarly, in tests containing sodium, no reaction with the steel was observed.

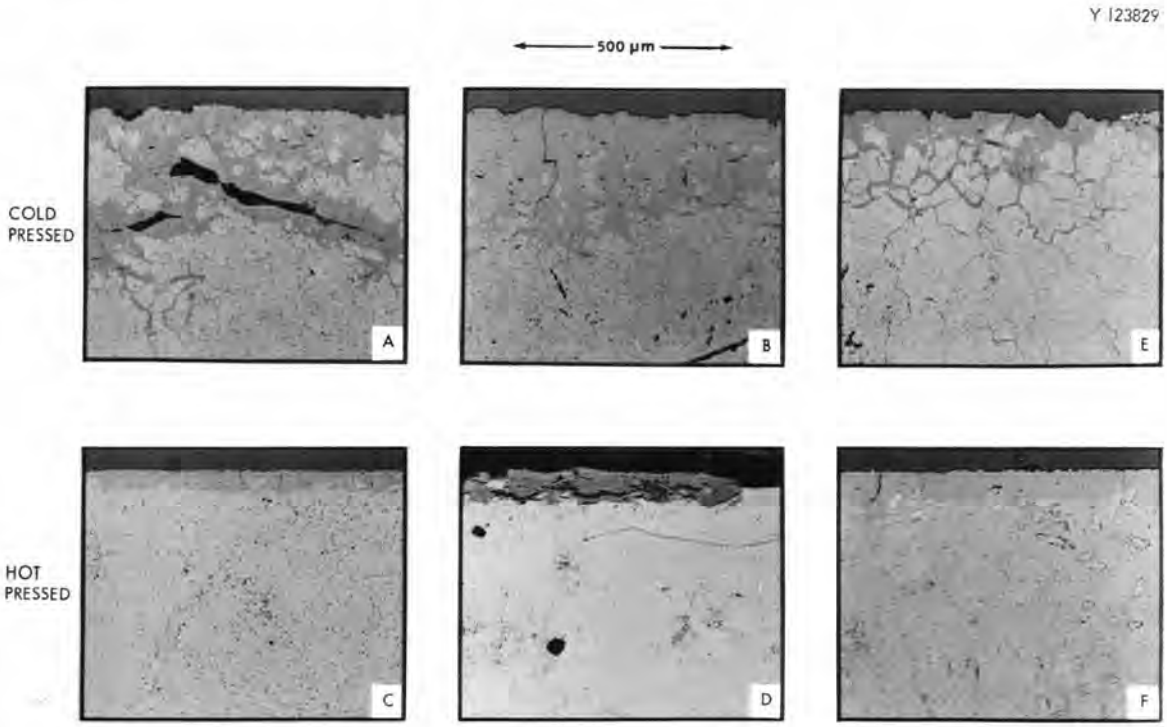

Fig. 6. Eu_2O_3 exposed to sodium and type 316 stainless steel for 1000 hr at 760°C. Top row, several cold-pressed pellets. Bottom row, several hot-pressed pellets.

IRRADIATION BEHAVIOR

The ultimate proof of suitability of a potential absorber material requires satisfactory performance under actual reactor operating conditions. Hence, a significant part of our program has been directed toward obtaining irradiation experience with Eu_2O_3 in a sodium-cooled fast reactor. Specifically, we have inserted three separate test assemblies into the EBR-II (Experimental Breeder Reactor-II). These are designated BICM-1 and BICM-2 (Instrumented Control Materials) and FDOT (Fast Test Reactor Design-Oriented Irradiation Test). A complete description of the BICM-1 experiment and its results have

been published,[27] as well as a detailed description,[28] and results[29] from the first- and second-stage irradiation of FDOT. The BICM-2 experiment has recently completed exposure, while the third-stage portion of FDOT is still undergoing irradiation.

BICM-1 Experiment

The BICM-1 experiment contained eight Eu_2O_3 pellets: four of cubic phase hot-pressed material (92% dense), two of monoclinic phase hot-pressed material (94% dense), and two of monoclinic phase sintered material (95% dense). These pellets were irradiated in an instrumented assembly allowing continuous pellet centerline temperature monitoring. The time- and volume-averaged temperature of all pellets was about 700°C. Irradiation during approximately an 18-month span resulted in accumulation of a fluence of 6×10^{22} neutrons/cm^2 ($E > 0.11$ MeV). Results of the post-irradiation examination can be summarized as follows:

1. **Hot-pressed cubic Eu_2O_3.** The four cubic pellets densified from a pre-irradiation average of 92.3 to an average of 94.4% of theoretical density during irradiation. Their diameters decreased 0.5% and they exhibited chipped edges, as shown in Fig. 7. It is not known whether chipping occurred before irradiation from shipping and handling, during irradiation, or after irradiation from shipping and handling. The diametral shrinkage and resultant density increase was most likely not due to

27. M. M. Martin, A. E. Pasto, and R. G. Donnelly, *Irradiation Behavior of Eu_2O_3 in EBR-II Experiment BICM-1*, ORNL-5096, Oak Ridge (January 1976).

28. M. M. Martin, A. E. Pasto, J. W. Woods, and R. G. Donnelly, *Description of FTR Design-Oriented Irradiation Test of Eu_2O_3 in EBR-II*, ORNL/TM-4996, Oak Ridge (November 1975).

29. M. M. Martin, *Performance of Eu_2O_3 in FTR Design-Oriented Irradiation Test in EBR-II*, ORNL/TM-5400, Oak Ridge (June 1976).

R-70228

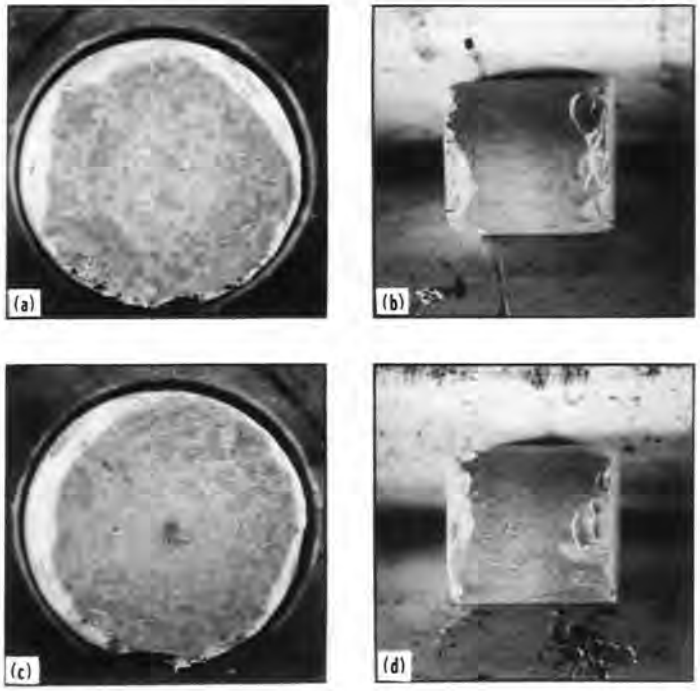

Fig. 7. Hot-pressed cubic Eu_2O_3 pellet. (a) and (c) Top and bottom surfaces, respectively, 10×. (b) and (d) Side surfaces, 6×. Reduced 20%.

transformation to the denser monoclinic phase, since x-ray diffraction revealed crystalline material with no evidence of diffraction lines attributable to the monoclinic structure. The shrinkage has tentatively been ascribed to a sintering effect associated with the atomic displacement processes occurring in the reactor core, since examination of the microstructure showed that the amount of fine porosity initially present in the pellets decreased upon irradiation (compare Fig. 8 top and bottom).

2. **Hot-pressed monoclinic Eu_2O_3.** The density of the two hot-pressed monoclinic pellets decreased from 94.4 to 87.6% of theoretical density during irradiation. Their diameters increased 3.9% and they exhibited axial and a few circumferential cracks that can be clearly seen in Fig. 9. X-ray diffraction patterns revealed crystalline material of the monoclinic structure.

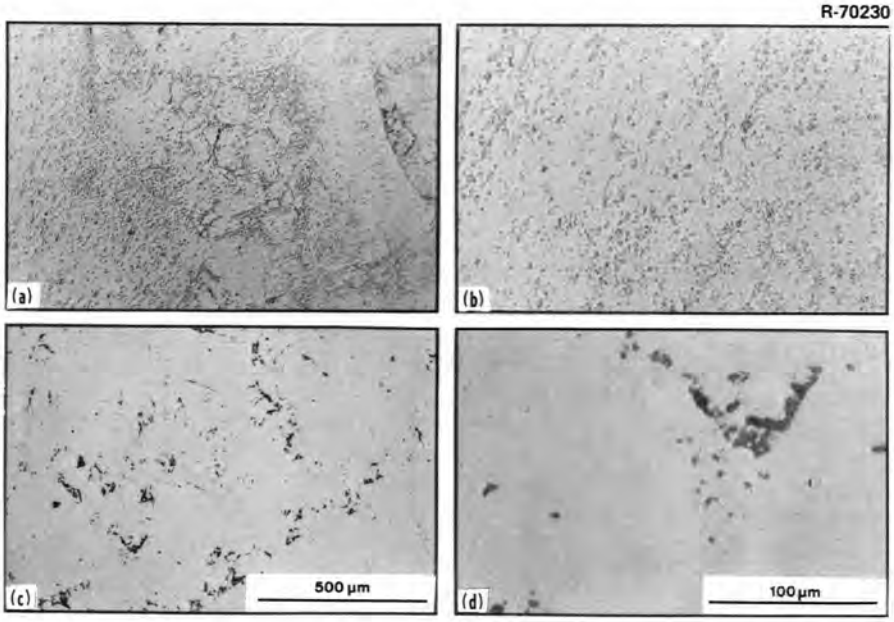

Fig. 8. Microstructure of polished specimens of cubic Eu_2O_3. Top row, unirradiated. Bottom row, irradiated. (a,c) 100×. (b,d) 500×.

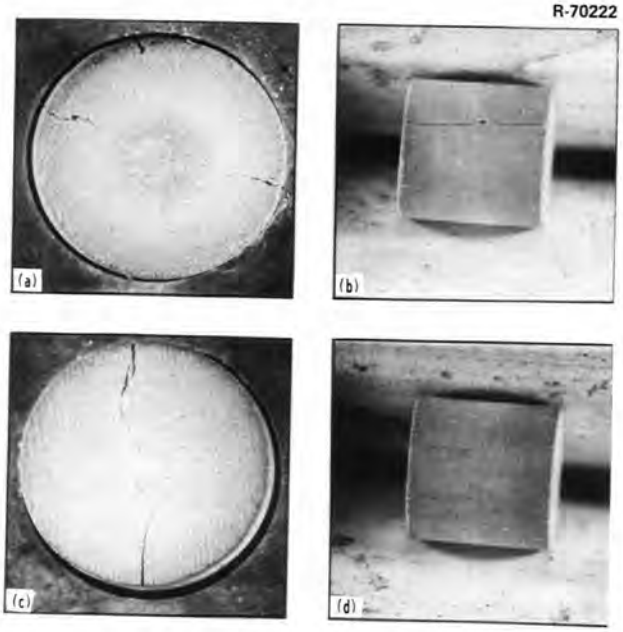

Fig. 9. Hot-pressed monoclinic Eu_2O_3 pellet. (a) and (c) Top and bottom surfaces, respectively, 10×. (b) and (d) Side surfaces, 6×. Reduced 30%.

3. **Sintered monoclinic Eu_2O_3.** The irradiation behavior of this material was similar to that of the hot-pressed monoclinic europia. During irradiation, the density of the two pellets decreased from 95.4 to 90.8% of theoretical density. Their diameters increased 3.6% and they exhibited both axial and many circumferential cracks, again clearly visible in Fig. 10.

The microstructures of the two different types of monoclinic pellets before and after irradiation are shown in Fig. 11. Note that the sintered europia had a significantly greater initial grain size, but that this did not seem to significantly affect the irradiation behavior.

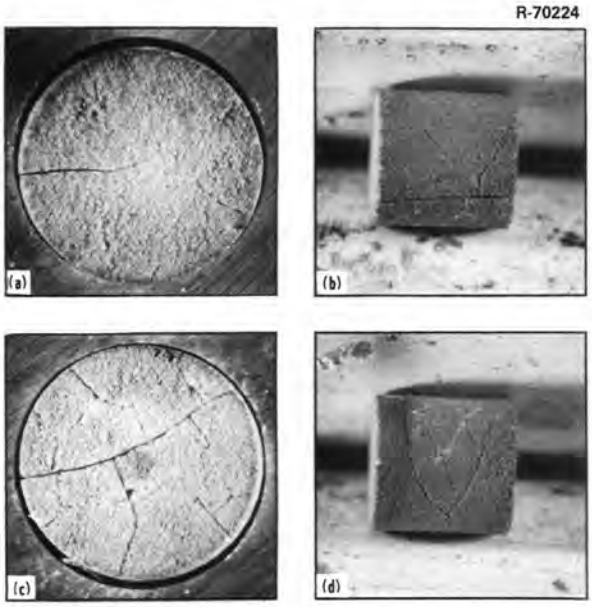

Fig. 10. Sintered monoclinic Eu_2O_3 pellet. (a) and (c) Top and bottom surfaces, respectively, 10×. Reduced 31%. (b) and (d) Side surfaces, 6×. Reduced 31%.

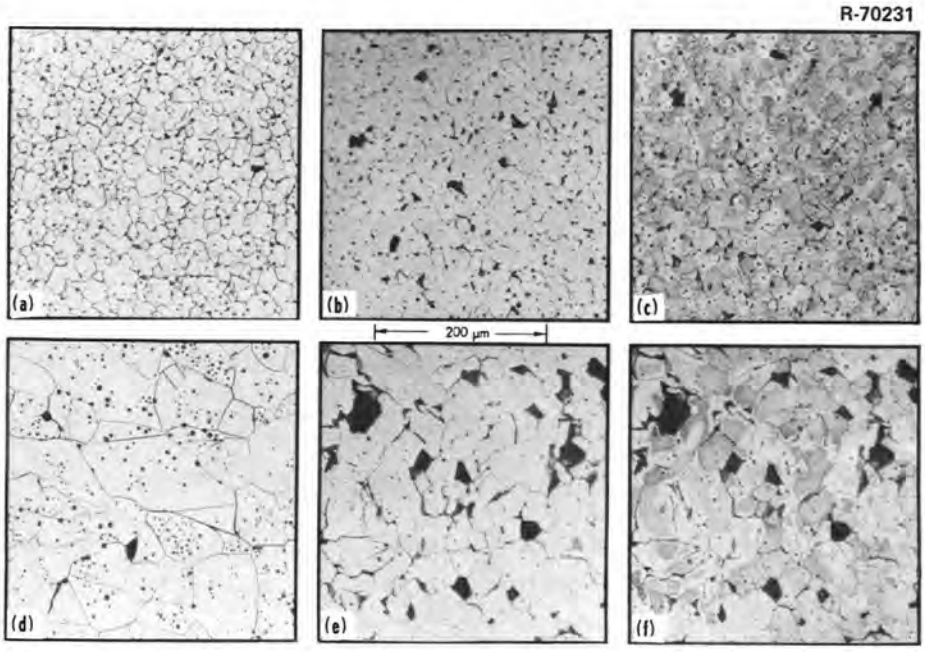

Fig. 11. Microstructure of polished and etched specimens of monoclinic Eu_2O_3. Top row, hot-pressed. Bottom row, sintered. (a,d) Unirradiated. (b,e) Irradiated, slightly etched. (c,f) Irradiated, severely etched.

BICM-1 Experiment Conclusions

Based on the results of the post-irradiation examination, the BICM-1 irradiation behavior can be summarized as follows:

1. The observed in-reactor densification of cubic Eu_2O_3 resulted primarily from the elimination of a portion of the initial porosity present in the as-fabricated pellets as a consequence of irradiation-induced sintering.
2. The monoclinic pellets exhibited a density decrease during irradiation, which was enhanced by the formation of intergranular microcracks. Thermal stresses, which contributed to the formation of the microcracks, also produced axial macrocracks.
3. The irradiation performance of monoclinic Eu_2O_3 was not dependent on grain size in the range of 16 to 300 μm, as evidenced by the similarity of observed axial cracks in both hot-pressed and sintered europia. The hot-pressed europia of smaller grain size showed less circumferential cracking than the sintered material of larger grain size.
4. Both monoclinic and cubic phase Eu_2O_3 pellets exhibited characteristic x-ray diffraction patterns, indicating that their crystal structures were retained intact.
5. Eu_2O_3 is compatible with 316 stainless steel in a fast-neutron environment to temperatures of at least 725°C.

FDOT Experiment Results

The FDOT experiment contained three stages, designed to give nominal exposures in EBR-II of six months in row 8, six months in row 8 plus one month in row 2, and 34 and 40 months in row 8. This irradiation schedule provided various fluences, temperatures, and stresses on the pellets, as described below. The experiment tested 223 pellets included in 23 separate container pins in 11 capsules. The test variables are summarized in Table 9. All pins contained europia pellets in stainless steel using helium as the heat transfer medium – except for pin 0-31T1, which contained sodium in contact with the pellets.

Post-irradiation examination of the six- and seven-month exposure pellets is now complete. The accumulated fast-neutron fluences (>0.11 MeV) were 8 and 18 $\times$ 10^{21} neutrons/cm^2, respectively. During the first-stage irradiation in row 8, the in-core test specimens experienced beginning-of-life volumetric average temperatures and outer surface tangential stresses that ranged respectively from about 730°C and 380 MPa (55,000 psi) for large-diameter monoclinic to 540°C and 80 MPa (12,000 psi) for small-diameter cubic pellets. Similar values for the more severe conditions of the second stage, which was subsequently conducted in row 2 with only large-diameter monoclinic pellets, were about 1080°C and 790 MPa (115,000 psi). Results of the post-irradiation examination can be summarized as follows:

1. Eleven pins with a total of 103 Eu_2O_3 test pellets were included in the first- and second-stage irradiations. Following irradiation, no significant changes were observed in the outer diameter of the type 316 stainless steel tubing.
2. **Small-diameter sintered monoclinic Eu_2O_3.** The 11 helium-bonded and 5 sodium-bonded type A pellets irradiated in the first stage were free of obvious defects such as macrocracks and chipped edges. Their diameters increased, on the average, by 0.06 and 0.13%, respectively. However, the sodium-bonded pellets apparently lost oxygen, as evidenced by their uniformly darker surfaces. The temperature was about 454°C during this experiment. No reaction product due to contact of europia with sodium was detected, but sodium did penetrate into the interior of the pellets.

Table 9. Summary of variables for Eu_2O_3 irradiation test in EBR-II

Capsule	Pin	Eu_2O_3 phase	Consolidation technique	Grain size (μm)	Density (% of theoretical)	Eu_2O_3 pellet diameter[a] (in.)	(mm)	Nominal test duration (months)
0-28	0-28T	Monoclinic	Sintered	>20	95 ± 1	0.63	16.0	6
	0-28B	Monoclinic	Sintered	<20	94 ± 1	0.63	16.0	6
0-29	0-29T	Monoclinic	Sintered	<20	94 ± 1	0.50	12.7	6
	0-29B	Cubic	Hot-pressed	<10	90 ± 2	0.50	12.7	6
0-30	0-30T	Cubic	Hot-pressed	<10	90 ± 2	0.63	16.0	6
	0-30B	Monoclinic	Sintered	<20	94 ± 1	0.63	16.0	6
0-31	0-31T1	Monoclinic	Sintered	<20	94 ± 1	0.50	12.7	6
	0-31T2	Monoclinic	Sintered	<20	94 ± 1	0.63	16.0	6
	0-31B	Monoclinic	Hot-pressed	<20	94 ± 1	0.63	16.0	6
0-32	0-32T	Monoclinic	Sintered	<20	94 ± 1	0.63	16.0	40
	0-32B	Cubic	Hot-pressed	<10	90 ± 2	0.63	16.0	40
0-33	0-33T	Monoclinic	Sintered	<20	94 ± 1	0.50	12.7	40
	0-33B	Monoclinic	Sintered	<20	94 ± 1	0.63	16.0	40
0-34	0-34T	Monoclinic	Sintered	<20	94 ± 1	0.63	16.0	*b*
	0-34B	Monoclinic	Hot-pressed	<20	94 ± 1	0.63	16.0	*b*
0-35	0-35T	Monoclinic	Sintered	>20	95 ± 1	0.63	16.0	34
	0-35B	Monoclinic	Sintered	<20	94 ± 1	0.63	16.0	34
0-36	0-36T	Cubic	Hot-pressed	<10	90 ± 2	0.63	16.0	34
	0-36B	Cubic	Hot-pressed	<10	90 ± 2	0.63	16.0	34
0-37	0-37T	Monoclinic	Sintered	<20	94 ± 1	0.63	16.0	34
	0-37B	Monoclinic	Hot-pressed	<20	94 ± 1	0.63	16.0	34
0-38	0-38T	Monoclinic	Sintered	<20	94 ± 1	0.63	16.0	34
	0-38B	Monoclinic	Sintered	<20	94 ± 1	0.50	12.7	34

[a]Length of pellet is twice its diameter.
[b]Six months in row 8 plus one month in row 2.

3. **Large-diameter sintered monoclinic Eu_2O_3.** (a) The irradiation testing of this 1650°C-sintered material in the first stage included 31 test specimens. Inspection of these pellets following the test revealed that the pellets usually contained one axial macrocrack, whose radial depth decreased with increasing distance of the subject pellet from the midplane of the reactor core. Thermally-induced stresses during irradiation testing caused the formation of these cracks. A sample crack is shown in the pellet in Fig. 12. The small but definite decrease in geometric density of the test pellets was also a function of distance from the core midplane. Similarly, swelling of the nine pellets irradiated in the first reactor exposure and later in the more severe second exposure in row 2 of the EBR-II depended strongly upon their vertical location in the pin. In this case, swelling as measured by changes in geometric density varied between 2.2 and 1.4% among the first through the fifth pellets in the stack and then decreased to <0.6% for the remaining four above the active core. In terms of dimensions, the diameter and length changes were respectively 0.70 and 0.73% for the first pellet, 0.48 and 0.55% for the fifth pellet, and <0.3 and 0.3% for the remainder. The first through the fifth pellets exhibited both axial and circumferential macrocracks; the sixth and seventh each had one shallow axial macrocrack; and the eighth and ninth were free of obvious defects.

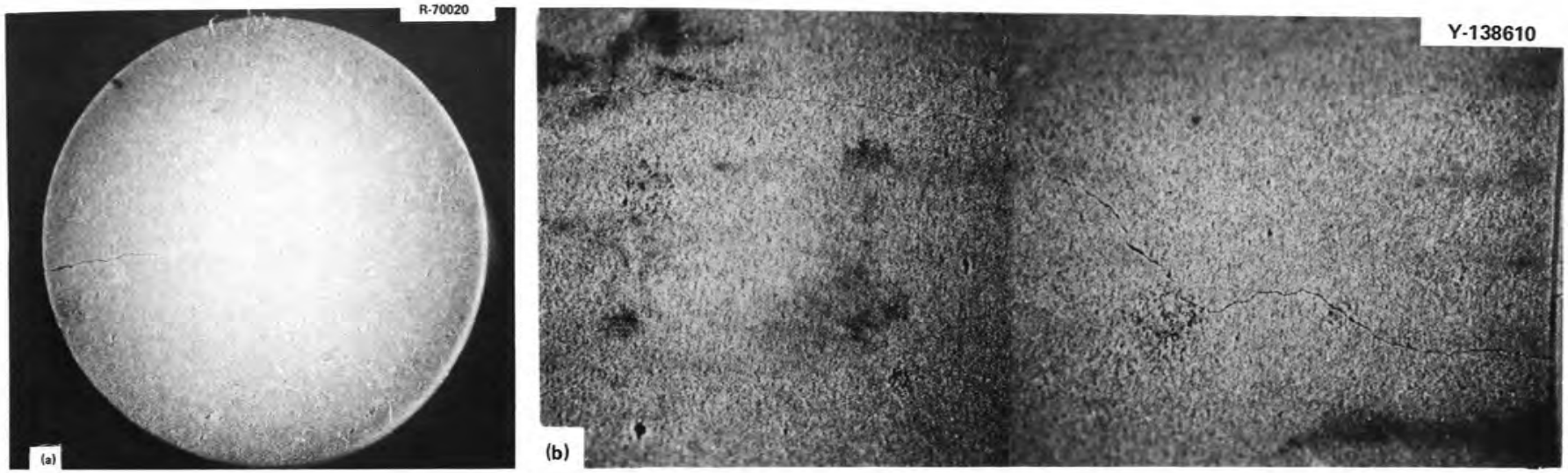

Fig. 12. Macrostructure of 0-30B-1 pellet Type D, 7×. (a) Top surface. Reduced 38%. (b) Portion of circumferential surface. Reduced 6%.

(b) The row 8 irradiation behavior of the nine 1750°C-sintered monoclinic Eu_2O_3 pellets of about 27-μm (1060-μin.) grain size was similar to that of 1650°C-sintered material having an initial grain size of about 13 μm. That is, most of the former pellets exhibited one axial macrocrack, and their overall growth averaged only 0.14% in diameter and 0.10% in length during first-stage irradiation. Before irradiation, both products contained microcracks up to several hundred micrometers in length. The thermal stresses that developed during irradiation produced additional microcracks and/or extended the length of cracks initially present. This effect was more pronounced in the pellets which initially had the larger grains.

4. **Hot-pressed monoclinic Eu_2O_3.** The nine pellets of this type that were irradiated only in the first stage showed little, if any, swelling, but they did exhibit many axial and circumferential macrocracks resulting from thermally-induced stresses. Seven emerged intact from the pin, as shown in Fig. 13. The other two were cleanly broken into half and quarter sections. The additional and more severe exposure of the second-stage irradiation caused further deterioration of the physical integrity of this material. These nine Eu_2O_3 specimens contained numerous axial and circumferential macrocracks that had formed during irradiation, and six had fragmented into three or more pieces. This type of behavior is shown in Fig. 14.

Fig. 13. Appearance of whole type F Eu_2O_3 pellets from pin 0-31B, 1.7×. Reduced 45%.

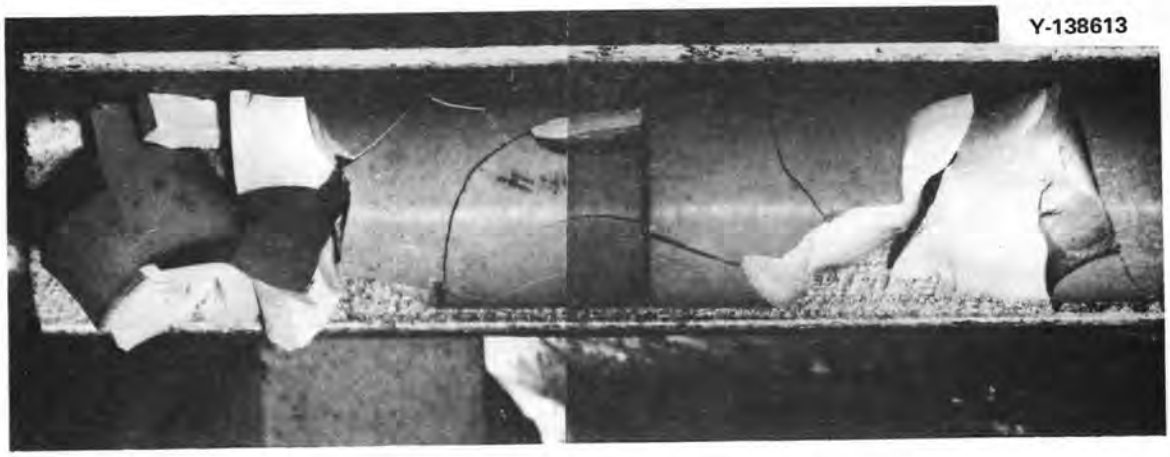

Fig. 14. Appearance of type F Eu_2O_3 pellets from pin 0-34B, 3×. Reduced 8%. Left and right: First and second pellets from midplane of reactor core during irradiation.

The fragments and three intact pellets, however, did not interact mechanically with the cladding and/or each other, as evidenced by the retained surface finish on the inside surface of the cladding, lack of Eu_2O_3 powder within the pin, and the ease with which pellets were removed from the pin. For those pellets which could be measured, diameters increased only about 0.6%. No evidence of formation of microcracks was detected.

5. **Hot-pressed cubic Eu_2O_3.** The eleven smaller and nine larger cubic phase pellets in the experiment swelled slightly during irradiation in row 8. Their diameters increased about 0.2% and most exhibited conchoidal chipping of the edges as shown in Fig. 15. The europia fragments resulting from chipping became wedged in the 2% diametral gap in the pins and severely hindered removal of both types of specimens from the assemblies. However, all of these specimens were free of thermally-induced macro- and microcracks. Also, the before- and after-irradiation microstructure of this product contained the same level of submicron size porosity, although a reduction was anticipated based on our early BICM-1 results. No evidence of either chemical incompatibility or deleterious mechanical interaction between cubic Eu_2O_3 and type 316 stainless steel cladding was detected.

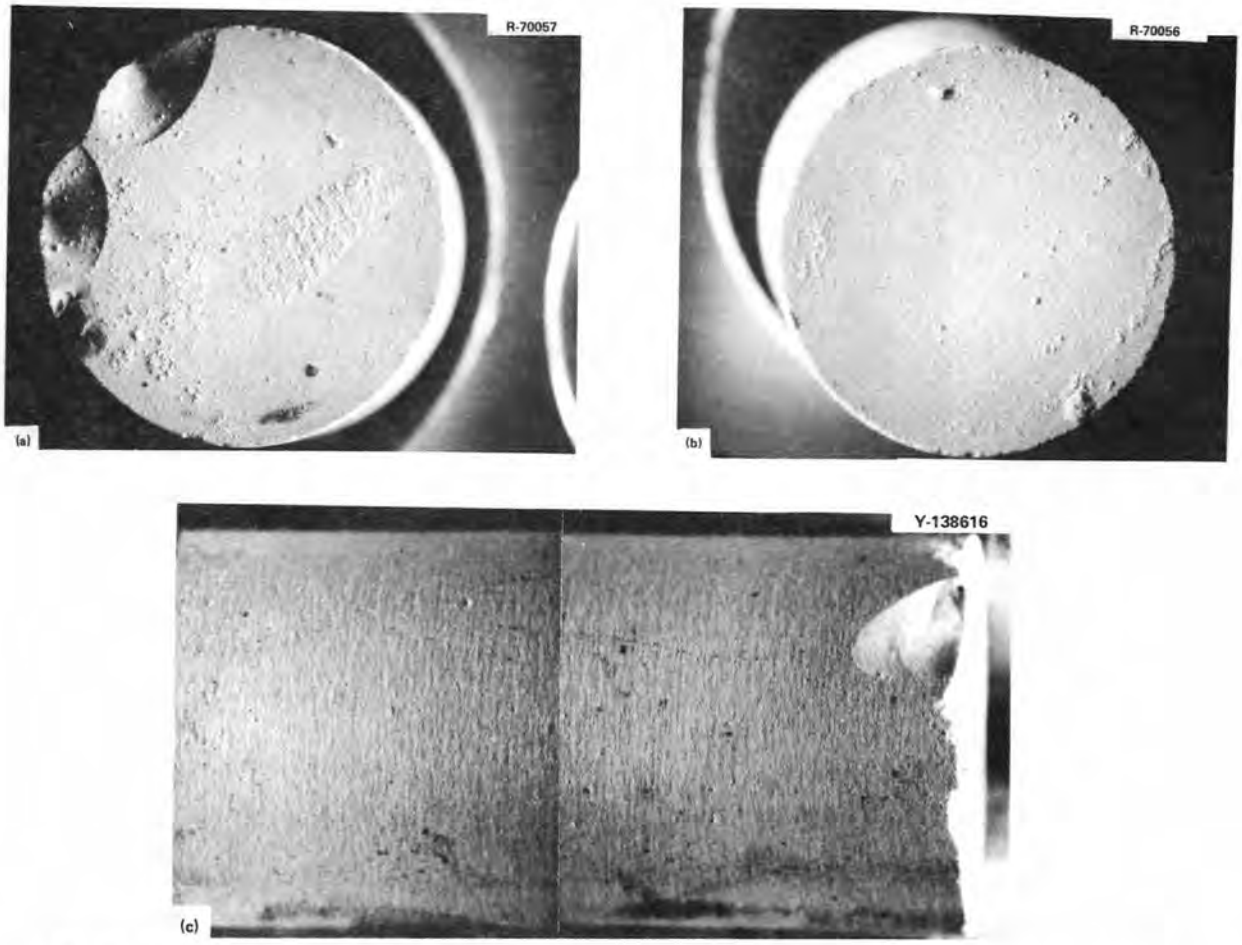

Fig. 15. Macrostructure of pellet 0-29B-2, 8×. (a) Top surface. Reduced 46%. (b) Bottom surface. Reduced 47%. (c) Portion of circumferential surface. Reduced 31%.

FDOT Experiment Conclusions

Based on the results of the FDOT post-irradiation examination, the following conclusions are offered:

1. A fast-neutron (>0.11 MeV) fluence of up to 8×10^{21} neutrons/cm^2 in row 8 of the EBR-II causes little, if any, swelling of the FDOT Eu_2O_3 materials. Similarly, the additional exposure of both hot-pressed and sintered monoclinic test pellets in row 2, which accumulated a total fast-neutron fluence of up to 18×10^{21} neutrons/cm^2, produced no significant swelling.
2. The slight increase in dimensions of the monoclinic Eu_2O_3 test pellets results primarily from formation of axial and circumferential intergranular macrocracks during irradiation. Cracking occurred predominantly in in-core pellets that were subjected to higher thermal stresses than those either above or below the active core. Their maximal change in diameter was, respectively, <0.4 and <0.8% for the exposure in rows 8 and 2.
3. A higher operating temperature requires a higher thermally-induced tangential stress to produce macrocracks in monoclinic Eu_2O_3. Apparently, the conditions for the formation of macrocracks in this material are surface stresses of >300 and >650 MPa (43,000 and 94,000 psi) for volumetric pellet temperatures of about 730 and 1080°C, respectively. The peak operating conditions for the cubic Eu_2O_3 test pellets were about 660°C and 185 MPa (27,000 psi), and under these conditions all pellets were free of macrocracks.
4. The hot-pressed cubic pellets failed to densify during irradiation, contrary to earlier BICM-1 results on similar material exposed at a comparable temperature but for a longer period of 18 months and a higher fluence of 60×10^{21} neutrons/cm^2. The pellet diameters increased, on the average, <0.2%; and, in contrast to monoclinic Eu_2O_3 behavior, these changes were independent of vertical location in the pin. Apparently, the threshold for in-reactor sintering of hot-pressed cubic products requires either a fast-neutron fluence greater than 8×10^{21} neutrons/cm^2, a longer period than five months at temperature, or both.
5. The irradiation performance of monoclinic Eu_2O_3 was unaffected by grain size differences in the range of 8 to 27 μm.
6. The intergranular microcracks that were present in sintered monoclinic Eu_2O_3 before irradiation improve the physical integrity of this product during irradiation. These defects provide sites to relieve stresses from anisotropic growth of the basic monoclinic crystallites and to arrest continuing formation of macrocracks from thermal gradients. For example, the large-diameter sintered pellets usually contained only one axial macrocrack after irradiation in row 8. However, the hot-pressed monoclinic pellets, which were free of microcracks, formed many axial and circumferential macrocracks during reactor exposure. The additional exposure to the more severe conditions in row 2 resulted in further deterioration of both products; but most of the sintered pellets remained intact, while hot-pressed material usually fragmented into three or more large pieces.
7. Sodium penetrates readily into the interior of sodium-bonded sintered monoclinic Eu_2O_3 of 93% theoretical density during fast-neutron irradiation at an average volumetric temperature of about 505°C. The pellets maintained their physical integrity, and no significant chemical reaction occurred between the europia and the sodium. However, if this condition existed in an operating Eu_2O_3-bearing control rod that would experience a rapid temperature rise, the entrapped sodium could conceivably cause severe swelling of the affected pellets due to thermal expansion of the sodium and possible resultant rupture of the cladding.
8. Both cubic and monoclinic Eu_2O_3 are compatible with type 316 stainless steel under fast-neutron irradiation to temperatures of at least 650°C.

It is apparent from our irradiation tests, that Eu_2O_3 has desirable properties as a solid neutron absorber material up to a fluence of 6×10^{22} neutrons/cm^2 ($E < 0.11$ MeV) at an average pellet temperature near 700°C. Further data are required at higher flux levels characteristic of fast test reactors in order to determine if the good performance characteristics observed at flux levels typical of EBR-II are also observed at neutron fluxes more typical of anticipated commercial LMFBRs.

SUMMARY AND RECOMMENDATIONS

We have found no experimental evidence to indicate that monoclinic Eu_2O_3 would be unsuitable for fast reactor application as a control rod material. Pellets crack during irradiation, as expected from thermal stress calculations and the thermal performance tests, but this cracking does not appear to be detrimental to control assembly performance. The oxide is chemically compatible with the cladding at anticipated operating temperatures, both inside and outside the core. Radiation swelling appears to be a function of temperature, flux, and/or fluence in a manner which is not presently well understood. It is in this area that critical future studies are required. This is especially true given the difference between the neutronic environment of our test pellets in EBR-II and those of anticipated demonstration and commercial LMFBRs. Determination of other physical properties of irradiated pellets, such as elastic moduli, thermal conductivity and expansion, etc., would provide data very useful in absorber assembly design.

The cubic phase europia has a slightly different set of thermal and mechanical properties, with the result that cracking of the pellets is not observed during irradiation. However, edge chipping may lead to serious problems of mechanical interaction with the cladding. Further, high-fluence irradiation caused shrinkage of cubic phase material, an effect which would increase the pellet temperatures by causing an increase in the pellet-to-clad gap. This could conceivably accelerate the process of temperature increase, until the phase transformation temperature is surpassed, at which point a large volume contraction (>9%) would occur. The overall effect would be significantly higher temperatures in the pins than allowed in the original design. Such a sequence of events could result in significant problems concerning chemical compatibility with the cladding. Thus, the irradiation behavior of cubic europia would require significantly more study if this is to be a serious candidate material.

ACKNOWLEDGMENTS

The authors wish to acknowledge the many contributions to the success of the program from R. G. Donnelly, who served as principal investigator for the Advanced Absorber Program and group leader for the Ceramic Development Group during the tenure of the phases described in the report. We are indebted to the following for completion of several critical subtasks: R. K. Williams for thermal performance testing, T. G. Godfrey for thermal conductivity measurement, J. R. DiStefano for compatibility testing, and J. W. Woods for FDOT experiment assembly and irradiation test coordination.

ORNL-5291
Distribution Categories
UC-79b, 79e

INTERNAL DISTRIBUTION

1–3. Central Research Library
4. ORNL Y-12 Technical Library
5–7. Laboratory Records Department
8. Laboratory Records, ORNL RC
9. ORNL Patent Office
10. G. M. Adamson, Jr.
11. E. J. Allen
12. S. L. Bennett
13. E. E. Bloom
14. E. S. Bomar
15. G. W. Clark
16. J. A. Conlin
17. R. S. Crouse
18. F. L. Culler
19. J. E. Cunningham
20. J. H. DeVan
21. J. R. DiStefano
22–24. R. G. Donnelly
25. W. P. Eatherly
26. J. I. Federer
27. G. G. Fee
28. C. B. Finch
29. G. F. Flanagan
30. M. H. Fontana
31. U. Gat
32. T. G. Godfrey
33. W. O. Harms
34. L. A. Harris
35. R. L. Heestand
36. R. F. Hibbs
37–39. M. R. Hill
40. J. D. Holder
41. F. J. Homan
42. J. D. Jenkins
43. P. R. Kasten
44. T. S. Lundy
45–49. M. M. Martin
50. W. R. Martin (Y-12)
51. C. L. Matthews
52. D. L. McElroy
53. C. J. McHargue
54. C. S. Morgan
55. J. P. Moore
56. F. R. Mynatt
57–61. A. E. Pasto
62. P. Patriarca
63. H. Postma
64. A. C. Schaffhauser
65. J. L. Scott
66. R. R. Suchomel
67–69. V. J. Tennery
70. T. N. Tiegs
71. D. B. Trauger
72. G. C. Wei
73. J. R. Weir, Jr.
74. R. K. Williams
75. J. W. Woods
76. H. L. Yakel
77. C. S. Yust
78. R. W. Ballufi (consultant)
79. P. M. Buster (consultant)
80. W. R. Hibbard, Jr. (consultant)
81. H. Palmour III (consultant)
82. N. E. Promisel (consultant)
83. D. F. Stein (consultant)

EXTERNAL DISTRIBUTION

84–85. ERDA DIVISION OF REACTOR NUCLEAR RESEARCH AND APPLICATIONS, Washington, DC 20545
Director
86. ERDA IDAHO OPERATIONS OFFICE, P.O. Box 2108, Idaho Falls, ID 83401
Barry Smith
87. ERDA OFFICE OF PROGRAM MANAGEMENT, RESEARCH AND SPACE PROGRAMS, P.O. Box 81325, San Diego, CA 92138
J. B. Radcliffe

88. ERDA SAN FRANCISCO OPERATIONS OFFICE, 1333 Broadway, Wells Fargo Building, Oakland, CA 94612
    Manager
89–92. ERDA DIVISION OF WASTE MANAGEMENT, PRODUCTION AND PROCESSING, Washington, DC 20545
    Acting Assistant Director for Reprocessing
    Chief, Technology Branch
    Chief, Projects Branch
    Chief, Industrial Programs Branch
93–95. ERDA OAK RIDGE OPERATIONS OFFICE, P.O. Box E, Oak Ridge, TN 37830
    Director, Research and Technical Support Division
    Director, Reactor Division
    F. E. Dearing, Reactor Division
96–273. ERDA TECHNICAL INFORMATION CENTER, P.O. Box 62, Oak Ridge, TN 37830
    For distribution as shown in TID-4500 Distribution Categories
    UC-79b (Fuels and Materials) and UC-79e (Reactor Core Systems)

☆ U.S. GOVERNMENT PRINTING OFFICE: 1977-748-189/193